INTERNATIONAL JOURNAL OF HYDROGEN ENERGY XXX (2016) 1–10

Available online at www.sciencedirect.com

ScienceDirect

journal homepage: www.elsevier.com/locate/he

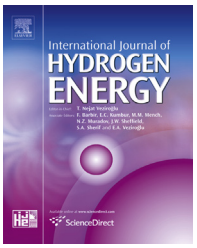

Performance analysis of the tracking of the global extreme on multimodal patterns using the Asymptotic Perturbed Extremum Seeking Control scheme

Nicu Bizon [a,b,*], Erol Kurt [c]

[a] Faculty of Electronics, Communications and Computers Science, University of Pitesti, 1 Targu din Vale, Arges, 110040 Pitesti, Romania

[b] University Politehnica of Bucharest, Doctoral School, Bucharest, Romania

[c] Faculty of Technology, Department of Electrical and Electronics Engineering, Gazi University, 06500 Teknikokullar, Ankara, Turkey

ARTICLE INFO

Article history:
Received 21 October 2016
Received in revised form
15 November 2016
Accepted 25 November 2016
Available online xxx

Keywords:
Extremum Seeking Control (ESC)
Photovoltaic (PV)
Partially Shaded Conditions (PSCs)
Global Maximum Power Point Tracking (GMPPT)
Multimodal pattern

ABSTRACT

This paper presents the capability of the Asymptotic Perturbed Extremum Seeking Control (aPESC) scheme to track the Global Extreme on multimodal patterns. The multimodal patterns are simulated based on power characteristics generated by a photovoltaic (PV) array under Partial Shading Conditions (PSCs). The aPESC scheme is tested to evaluate the performance of locating, searching and tracking of the Global Maximum Power Point (GMPP). The following performance indicators such as the searching resolution, tracking accuracy, tracking efficiency, and tracking speed are used to compare the performance of the GMPP tracking (GMPPT) algorithms. The aPESCH1 scheme proposed has been implemented in MATLAB/Simulink package to evaluate the performance indicators mentioned above. The results prove that the proposed aPESCH1 scheme is effective and simple to be implemented.

Introduction

The aPESC schemes were briefly introduced in Refs. [1–3] and its modeling, stability, and design rules were analyzed in Refs. [4,5]. According to literature, researches focus on the localization, searching and tracking of the Global Maximum Power Point (GMPP). The main performance indicators (searching resolution, tracking accuracy, tracking efficiency, and tracking speed [6–9]) will be evaluated in the present study for the proposed GMPPT algorithm.

The proposed GMPPT algorithm is compared with other GMPPT algorithms reported in the literature [6–9] to show its performance. Initially, the firmware-based GMPPT algorithms that are analyzed in reviews [6–9] operate in two stages, instead of the proposed GMPPT algorithm that may find the GMPP in one stage. Secondly, the firmware-based GMPPT

* Corresponding author.
E-mail addresses: nicubizon@yahoo.com, nicu.bizon@upit.ro (N. Bizon), ekurt52tr@yahoo.com, ekurt@gazi.edu.tr (E. Kurt).
http://dx.doi.org/10.1016/j.ijhydene.2016.11.173
0360-3199/

algorithms use in first stage advanced algorithms based on Fuzzy Logic Controller (FLC) [10], Artificial Neural Network (ANN) [11], Genetic Algorithms (GAs) [12], Differential Evolution (DE) [13], Particle Swarm Optimization (PSO) [14], or Ant Colony Systems (ACSs) [15]), and chaotic search [16]. However, after the GMPP is located, the GMPPT is tracked in the second stage using a classical MPPT algorithm such as Perturb and Observe (P&O) [17], Incremental Conductance (IC) [18], and Hill Climbing (HC) [19]. It is worth to mention that the classical MPPT algorithm may fail in tracking of GMPP, if the shading coefficient is over 30% or high variations appear on the irradiance profile [20,21]. So, the main objective of any GMPPT algorithm should be to track the GMPP under dynamic irradiance profile as in reality, quickly and accurately in order to increase the PV power generated with up to 45% in comparison with classical MPPT algorithms [22].

The main findings of this study are: (1) A systematic analysis of the aPESCH1 scheme is performed in order to estimate the tracking accuracy and the searching resolution of the GMPP on multimodal patterns; (2) The robustness of the GMPP searching on PV patterns under partially shaded conditions was shown using dynamic sequences of shaded PV power characteristics; (3) The tracking efficiency and tracking speed was estimated based on these dynamic sequences; (4) The robustness analysis to dither shape reveals that this is not important and the performance remains almost the same.

Some performance obtained are mentioned as follows: (1) Ability to discern the GMPP among the Local Maximum Power Points (LMPPs) is 20 times lower that 5% resolution reported by other GMPPT algorithms [6–9], (2) the average value of the tracking accuracy is of 99.97%, and (3) tracking speed is given by about 23 dither periods. The performance will be validated by the simulation results shown in sections below.

The paper is structured as follows: The PV characteristics of 1Px3S and 1Px5S arrays are shown in Section 2 under PSCs. The parameters of the solar cell and PV panel used in simulation are also mentioned here. Thus, a generic PV pattern is defined to be used in the simulation. In Section 3, the performance indicators (the searching resolution, tracking accuracy, tracking efficiency, and tracking speed) are defined. The results obtained for the performance indicators and robustness to irradiance profile with dynamical change of the PSCs, PV pattern with noise, and dither's shape are mentioned in Section 4. Finally, last section concludes the paper.

The scheme of aPESCH1 and power characteristics under partially shaded conditions

The robustness of the aPESCH1 scheme (see Fig. 1) are tested for rapid change of the shading coefficients for the PV irradiance profiles' sequences, noise on the PV irradiance profile, and use of different shapes for the dither signal.

The power characteristics generated by PV panels in series (S) and parallel (P) that are integrated into a large array of pPxsS structure, where p and s represent the number of panels that are connected in parallel and series, have multiple peaks if the panels are shaded. The power characteristics for PV array having the structure 1Px3S (top) and 1Px5S (bottom) are shown in Fig. 2 for different irradiance sequences.

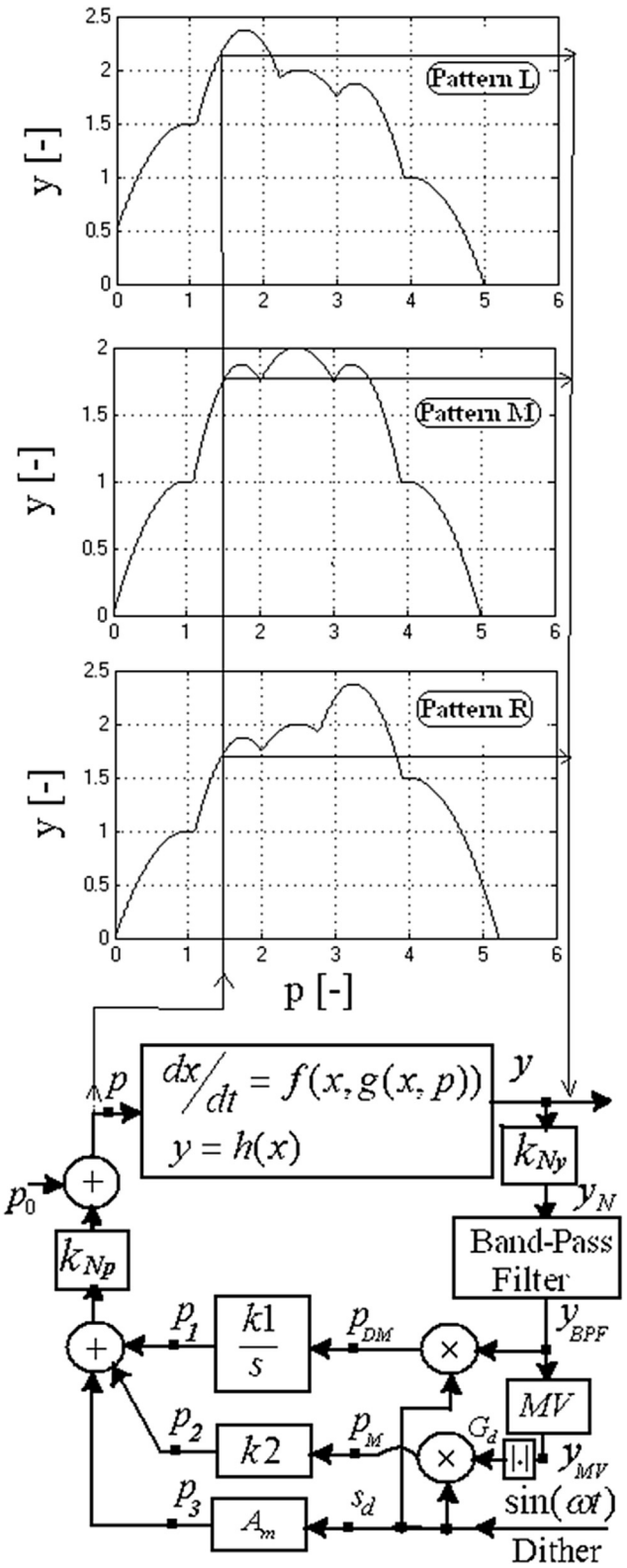

Fig. 1 – The aPESCH1 scheme and their operation using three shading patterns.

The functions, variables and parameters used in aPESCH1 scheme are the as following:

- the multimodal pattern is defined by function y = h(x),

Please cite this article in press as: Bizon N, Kurt E, Performance analysis of the tracking of the global extreme on multimodal patterns using the Asymptotic Perturbed Extremum Seeking Control scheme, International Journal of Hydrogen Energy (2016), http://dx.doi.org/10.1016/j.ijhydene.2016.11.173

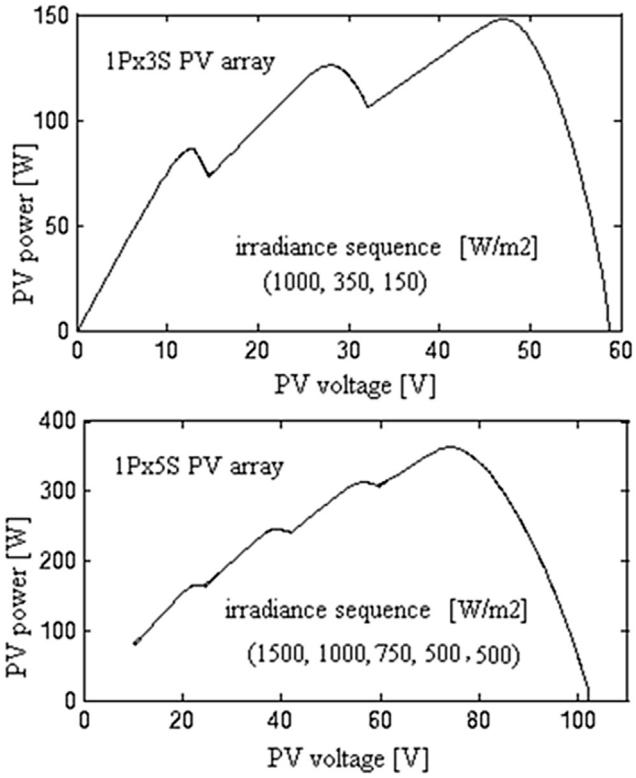

Fig. 2 – The power characteristics for PV array having the structure 1Px3S (top) and 1Px5S (bottom), and panels under different irradiance sequences.

$$y = h(x) = h(x_e(p)) = h(p); \tag{1a}$$

- the equilibrium point is defined by the smooth function x_e,

$$f(x,\ g(x,p)) = 0 \quad \Leftrightarrow \quad x = x_e(p), \tag{1b}$$

where p is the searching signal;

- the smooth function *f(x,u)* defines the system dynamic;
- the control law is *u(t)=g(x(t),p)*.

The variables and parameters used in aPESCH1 scheme and relations (2) below are as follows:

- the periodic dither s_d has the amplitude set to 1, and the frequency is $f_d = 1/T_d = \omega/2\pi$;
- the minimum dither has the amplitude A_m;
- the cut-off frequencies for the Band Pass Filter (BPF), $f_h = \beta_h \cdot f_d$ and $f_l = \beta_l \cdot f_d$, where β_h and β_l parameters will be set in range 0.1–0.9 and 1.5 to 5.5 in order to test the best compromise to design the BPF for a good approximation of the H1 harmonic and sufficient dither persistence on the control loop as well;
- the normalization gains, k_{Ny} and k_{Np}, are used to adapt the input and output signals of aPESCH1 scheme to used multimodal pattern without change the tuning parameters;
- the tuning parameters are the loop and dither gains, k_1 and k_2.

The relations (2) define the model of aPESCH1 scheme that are shown in Fig. 1:

$$y_N = k_{Ny} \cdot y, \quad y = f(x_1, x_2) \tag{2a}$$

$$\dot{y}_f = -\omega_h \cdot y_f + \omega_h \cdot y_N, \quad y_{HPF} = y_N - y_f, \quad \dot{y}_{BPF} = -\omega_l \cdot y_{BPF} + \omega_l \cdot y_{HPF} \tag{2b}$$

$$p_{DM} = y_{BPF} \cdot s_d, \quad s_d = \sin(\omega t), \tag{2c}$$

$$\dot{p}_{Int} = p_{DM} \tag{2d}$$

$$G_d = |y_{MV}|, \ \ y_{MV} = \frac{1}{T_d} \cdot \int y_{BPF} dt \tag{2e}$$

$$p_1 = k_1 \cdot p_{Int}, \ \ k_1 = \gamma_{sd} \cdot \omega \tag{2f}$$

$$p_2 = k_2 \cdot G_d \cdot s_d \tag{2g}$$

$$p_3 = A_m \cdot s_d, \tag{2h}$$

$$p = k_{Np} \cdot (p_1 + p_2 + p_3) + p_0, \tag{2i}$$

where (2a) to (2i) represent the static map, normalization, BPF filtering, demodulation, integration, computing of the gain dither (G_d), and p_1, p_2, and p_3 components of the searching signal (p). Note that p and y denote the input and output variables for the aPESCEH1 scheme, y_f is an intermediate variable related to HPF operating, p_{Int} is the output of the integration block, and the Mean Value (MV) block uses the Pade approximation to filter the y_{bpf} signal. The initial value of the scanning signal, p_0, is used in closed loop to estimate the level of harmonics in different points of the function y = h(x) (the PV power characteristic in case of Fig. 2).

In general, the large PV array operates under PSCs due to real environment conditions, because parts from the PV array installed on rooftop or/and facades of buildings or on ground may be shaded by the clouds, neighboring buildings, snow or dust [23]. Consequently, the power characteristics for such PV arrays would exhibit multiple LMPPs (Fig. 2).

The PV array uses PV module of SX60 type that is built as one column with 34 cells connected in series. Considering the one-diode model and neglecting the parallel resistance, R_p, the solar cell model is given by (3) [24]:

$$I_{PV(cell)} = K_{IG(cell)} \cdot G - I_{0R} \cdot \left[\exp\left(\frac{V_{PV(cell)} + R_s I_{PV(cell)}}{nV_T}\right) - 1\right] \tag{3}$$

where:

- $V_{PV(cell)}$ is the solar cell voltage;
- $I_{PV(cell)}$: the solar cell current;
- R_s: the series resistance of the solar cell;
- $K_{IG(cell)} = I_{sc(cell)}/G_R$: the irradiation to short-circuit current gain;

Please cite this article in press as: Bizon N, Kurt E, Performance analysis of the tracking of the global extreme on multimodal patterns using the Asymptotic Perturbed Extremum Seeking Control scheme, International Journal of Hydrogen Energy (2016), http://dx.doi.org/10.1016/j.ijhydene.2016.11.173

- $I_{L(cell)}=I_{sc(cell)}\cdot G/G_R$: the light-generated current;
- G: the irradiance's level;
- n: Diode ideality factor;
- I_{0R}: Reverse saturation current at reference temperature T_R;
- V_T: Thermic voltage;
- other parameters are defined in Table 1.

If the parameters of solar cell model and standard test conditions mentioned in Table 1 are used, then the open-circuit voltage, V_{oc}, and the short-circuit current, I_{sc}, of the SX60 panel will be about 21 V and 7.8 A. The MPP value will be about $P_{MPP} = 51{,}2$ W (obtained for $V_{MPP} = 14.63$ V and $I_{MPP} = 3.5$ A). If the irradiance level decreases at 500 W/m^2, then the power generated will decrease as well. Thus, the power generated depends by the irradiance level. The power generated by the PV panels can be increased if these are integrated in series (S) and parallel (P) into a large array of type pPxsS, where p and s represent the number of panels that are connected in parallel and series, respectively. The power characteristics for a PV array of 1Px3S and 1Px5S types are shown in Fig. 2. The irradiance sequences are mentioned in each case. It can be observed that multiple LMPPs appear on power characteristics. The PV pattern depends by the topology type used to implement the PV array, use or not of the bypass diodes for the PV panels, and the PSCs that may occur [25].

Different PV patterns will be obtained based on multimodal pattern (4) (three are shown in Fig. 1):

$$y = sat\left(L-(p-1)^2\right)+\text{sat}\left(M-(p-2.5)^2\right)+sat\left(R-(p-4)^2\right) \quad (4)$$

where the saturation function (*sat*) has the lower and upper limits set to zero and infinite and the (L, M, R) triplet set the position of the GMPP (in the left (1.5, 2, 1), middle (1, 2, 1), and right (1, 2, 1.5) side of the respective multimodal pattern shape of the multimodal pattern, see Fig. 1 – top).

Performance indicators

The performance indicators used to compare the GMPPT algorithms are the searching resolution, tracking accuracy, tracking efficiency, and tracking speed.

The searching resolution (S_R) is defined by (5) [6]:

$$S_R = \frac{\min_i |y_{GMPP} - y_{LMPPi}|}{y_{GMPP}} \cdot 100[\%] \quad (5)$$

The tracking accuracy (T_{acc}) is defined by (6):

$$T_{acc} = \frac{y_{GMPP}}{y^*_{GMPP}} \cdot 100[\%] \quad (6)$$

where y_{GMPP} is the global extreme and y^*_{GMPP} is the tracked value using a GMPPT algorithm.

So, the searching resolution is bonded by the tracking accuracy that can be obtained using a GMPPT algorithm:

$$S_R > 100 - T_{acc} \quad (7)$$

The tracking efficiency (T_{eff}) is given by (8):

$$T_{eff} = \frac{\int_0^t y dt}{\int_0^t y^* dt} \cdot 100[\%] \quad (8)$$

where y is the output of the multimodal pattern, and y^* is the current value tracked by a GMPPT algorithm.

The T_{eff} value is mainly dependent by the transitory accuracy during the searching phase, because the stationary accuracy is higher than 98% for most of GMPPT algorithms [6–9]. Thus, a short searching time may improve the tracking efficiency.

The tracking speed is defined by number of iterations until the global extreme is tracked with the imposed stationary accuracy. It is obvious that an iteration for the aPESC1 scheme means a dither period, but this can be defined for all GMPPT algorithms as the time to compute a specific function [9].

Simulation results

The values of the parameters used in simulation are the following: $f_d = 100$ Hz, $k_1 = 100\pi$, $k_2 = 3$, $p_0 = 0$, $k_{Ny} = 1$, and $k_{Np} = 3$. The cut-off frequency parameters of the BPF are set to $\beta_h = 0.5$ and $\beta_l = 5.5$. If it is not else mentioned, a sinusoidal dither with the amplitude of 1 V is used and the minimum dither amplitude, A_m, is set to 0.001 V.

Table 1 – Parameters of solar cell model.

Parameter	Description	Value [unit]
G_R	Reference irradiation	1000 [W/m^2]
T_R	Reference temperature	298 [K]
Q	Electron charge	1.6e^{-19} [C]
k_B	Boltzmann's constant	1.38e^{-23} [JK^{-1}]
N	Diode ideality factor	1.3 [-]
V_G	Silicon band-gap energy	1.12 [eV]
$V_T = k_B T_R/q$	Thermic voltage	26 [mV]
I_{0R}	Reverse saturation current at $T = T_R$	2e^{-9} [A]
α	Short-circuit current temperature coefficient	0.0025 [AK^{-1}]
R_s	Cell series resistor	3 [mΩ]
R_p	Cell shunt resistor	10 [Ω]
$V_{oc(cell)}$	Cell open-circuit voltage	0.61 [V]
$I_{sc(cell)}$	Cell short-circuit current	3.8 [A]

Please cite this article in press as: Bizon N, Kurt E, Performance analysis of the tracking of the global extreme on multimodal patterns using the Asymptotic Perturbed Extremum Seeking Control scheme, International Journal of Hydrogen Energy (2016), http://dx.doi.org/10.1016/j.ijhydene.2016.11.173

Tracking accuracy and searching resolution of the GMPP on static multimodal patterns

The simulation results for the proposed aPESCH1 scheme is shown in Figs 3–5 for the multimodal patterns that has the GMPP located in the left, middle, and right side of the respective multimodal pattern (see the top of Figs. 3–5). The structure of these Figures is the following: the PV pattern is shown on top; the output (*y*) is shown in the first plot; the asymptotic function (G_d) in the second plot; the searching signal (*p*) in third plot. The output of the aPESC scheme proposed in Ref. [2], y_{aPESC}, is also shown in the first plot. It can be observed that y_{aPESC} remains blocked in first LMPP located from the starting point $p_0 = 0$. Some zooms are shown to evaluate the performance indicators or validate the discussion above.

The tracking speed is about 12–15 iterations. The *p* signal scans the searching range of about 6 times to locate the GMPP and then this is accurately found during the next 6–9 iterations. Note that the average value of the tracking speed reported in Ref. [9] is in range 21 [26] to 473 [27]. The searching resolution is $S_R \cong 15.78\%$ (=0.375/2.375) for the pattern L and R, and $S_R \cong 6.25\%$ (=0.125/2) for the pattern M.

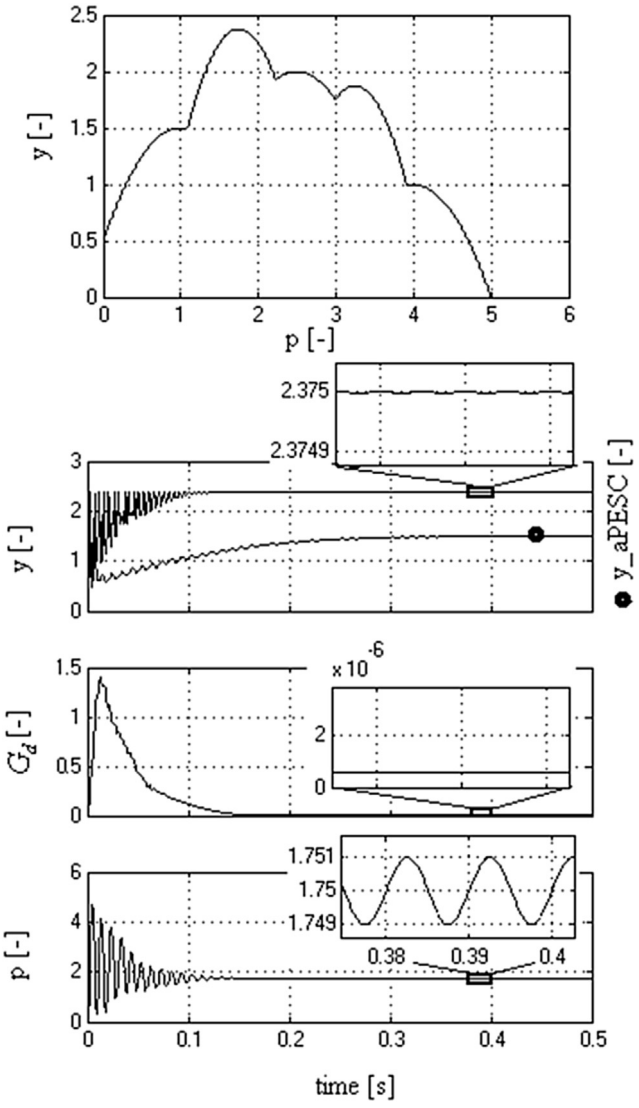

Fig. 3 – Tracking of the GMPP on the pattern L: (L, M, R) = (1.5, 2, 1).

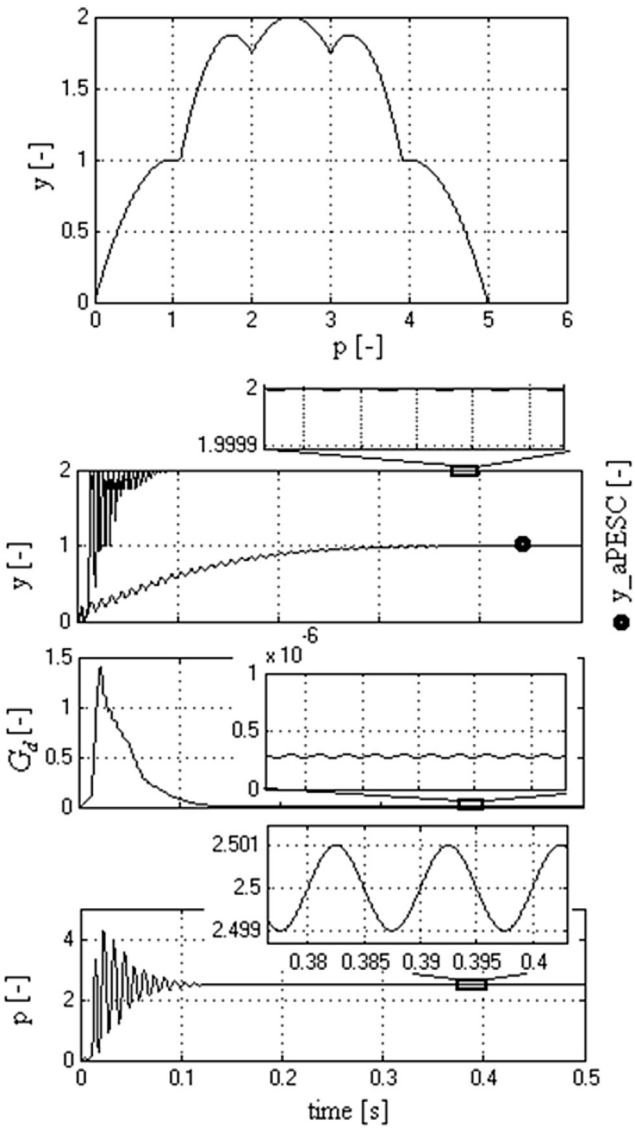

Fig. 4 – Tracking of the GMPP on the pattern M: (L, M, R) = (1, 2, 1).

The tracking accuracy is of 99.99% for all patterns based on the zooms shown for the y output. Considering (7), the searching resolution is higher than 0.01%. Also, note that the maximum value of the tracking accuracy reported in Ref. [9] for the PSO-based GMPPT algorithms is of 99.96%.

It is important to evaluate the $S_{R(100\%hit)}$ value, which is the resolution for 100% hit count. The value of hit count is defined as ratio of positive results of GMPP finding (instead of a LMPP) to total number of tests performed [9]. The $S_{R(100\%hit)}$ value is close to 100% for the PSO-based GMPPT algorithm [28] using PV pattern with $S_R \cong 4.36\%$. Note that 100% hit count may also be obtained the aPESCH1-based GMPPT algorithm using PV pattern with S_R lower that 6.25%. The simulation shown that 100% hit count may also be obtained for lower S_R that 6.25%, but higher than 0.25%.

Please cite this article in press as: Bizon N, Kurt E, Performance analysis of the tracking of the global extreme on multimodal patterns using the Asymptotic Perturbed Extremum Seeking Control scheme, International Journal of Hydrogen Energy (2016), http://dx.doi.org/10.1016/j.ijhydene.2016.11.173

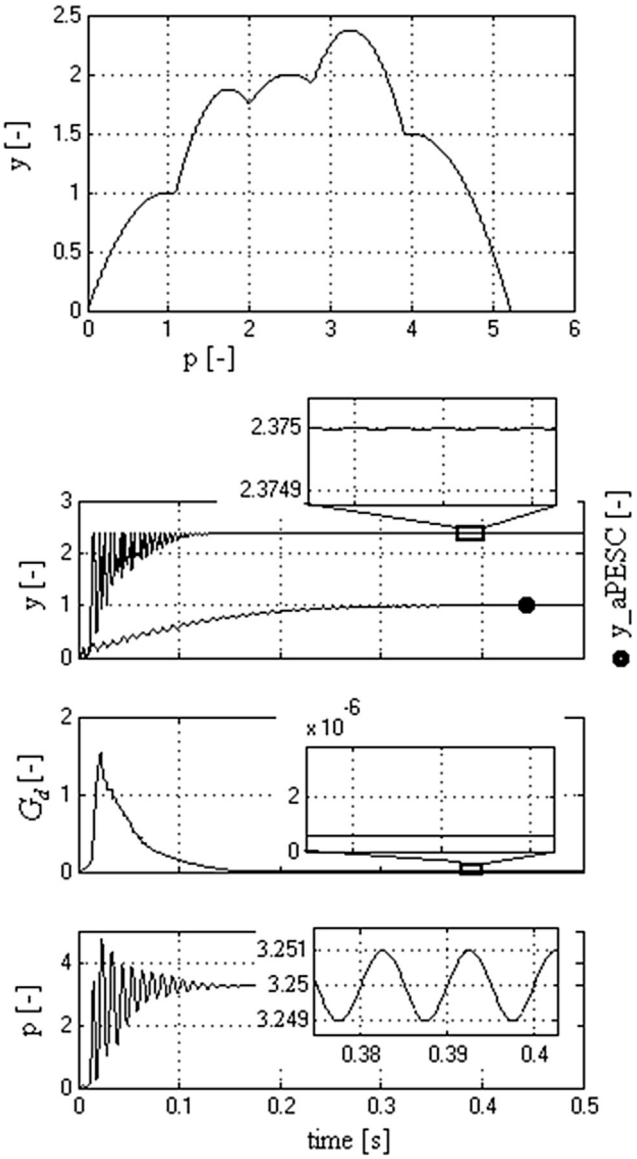

Fig. 5 – Tracking of the GMPP on the pattern R: (L, M, R) = (1, 2, 1.5).

The robustness of the GMPP searching

Robustness to irradiance profile with dynamical change of the PSCs

The robustness of the GMPP searching will be tested for a PV patterns' sequence with dynamical change of the PSCs defined by the combination of three PV patterns mentioned above (see Fig. 6).

The PV patterns (1.5, 2, 1), (1, 2, 1.5) and (1, 2, 1) are dynamically changed at each 0.2 s. The structure of the Fig. 6 is the following: the output (*y*) is shown in the top plot; the dither gain (G_d) is shown in the middle plot, and the searching signal (*p*) is shown in the bottom plot. The passing from one pattern to other is made dynamically at each 0.2 s. The dither gain (G_d) increases at each change to increase the searching gradient. It is observed that tracking of the GMPP is obtained in less or more iterations, depending by the order of the PV patterns in sequence.

Robustness to PV pattern with noise

If noise is added for example to the PV pattern R (1, 2, 1.5), then the GMPPs will be dependent by this level. The GMPP is located at (p, y) = (3.25, 2.375) for PV pattern R without noise, and close LMPP is located at (p, y) = (2.5, 2). Thus, the difference between the levels of GMPP and LMPP is of 0.373 (=2.375−2). If the level of noise is lower than 0.373, then $y_{GMPP} > y_{LMPP}$ and the current position of GMPP (y_{GMPP}) will be tracked (Fig. 7a).

If the level of noise is higher than 0.373, then y_{GMPP} may decrease to y_{LMPP} during some periods, when the current position of LMPP ($y_{LMPP} \cong 2$) will be tracked (Fig. 7c).

If the level of noise is around 0.373, then both cases may occur (Fig. 7b). It is worth to mention that global extreme is tracked in a few iterations. Note that noise is changed at each 10 ms (the sampling period of noise), so the current GMPP can be effectively tracked only if the dither frequency is set higher than 1000 Hz. Thus the dither frequency is important in setting the tracking search, but high frequency for the dither may interfere with the system dynamic. This aspect must be further analyzed. In this paper, only the effect of dither's shape will be analyzed in next section. Note that the output of the aPESC scheme proposed in Ref. [2], y_{aPESC}, is also shown in the first plot. It can be observed in Fig. 7a that y_{aPESC} remains blocked in first LMPP located from the starting point $p_0 = 0$, but for higher noise the aPESC scheme fails to track even this LMPP (see Fig. 7b and c).

Robustness to dither's shape

The robustness of the GMPP searching for dither with the period of 10 ms, but different shape is analyzed in this section (see Fig. 8). Note that this aspect was investigated in Ref. [29] for the aPESC scheme proposed in Ref. [2], and the

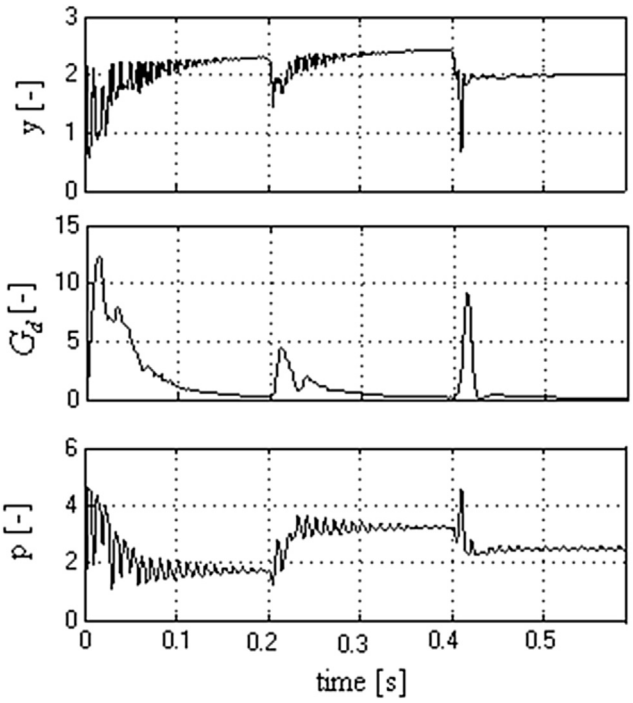

Fig. 6 – The robustness of the GMPP searching for the PV patterns' sequence: (1.5, 2, 1), (1, 2, 1.5) and (1, 2, 1).

Please cite this article in press as: Bizon N, Kurt E, Performance analysis of the tracking of the global extreme on multimodal patterns using the Asymptotic Perturbed Extremum Seeking Control scheme, International Journal of Hydrogen Energy (2016), http://dx.doi.org/10.1016/j.ijhydene.2016.11.173

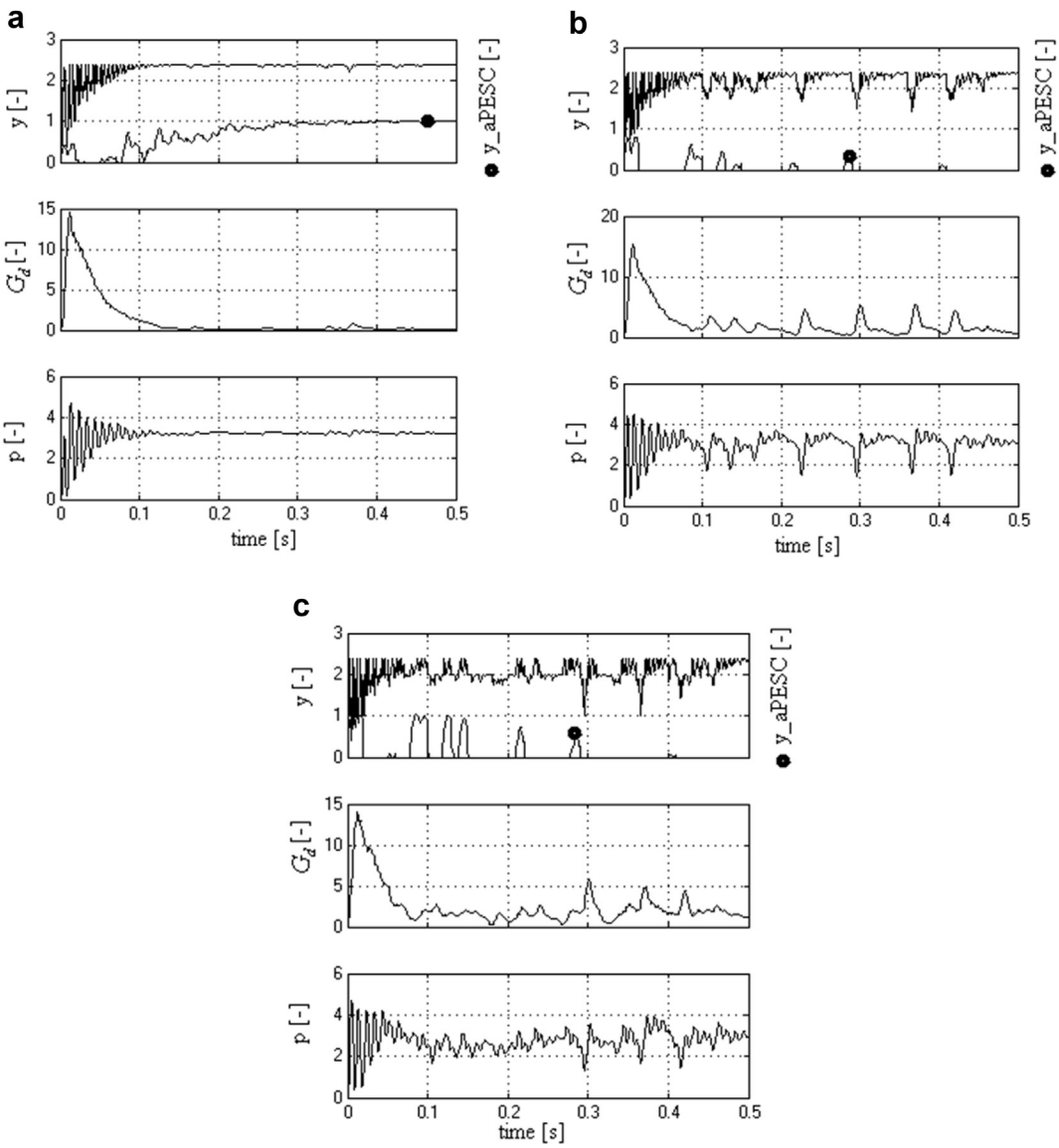

Fig. 7 – The robustness of the GMPP searching for the PV pattern R with random noise added on PV power. a. ±0.1 W random noise. b. ±0.3 W random noise. c. ±0.5 W random noise.

conclusion was that the shape of the dither is not important and the performance remains almost the same.

The following shape for the dither will be considered to validate this conclusion for aPESCH1 scheme proposed here as GMPPT algorithm: sinusoidal, rectangular, combination of sinusoidal and rectangular signals, saw-tooth, and random noise with sampling period of 10 ms.

It can be observed in Fig. 8 that the number of iterations necessary to find the GMPP of the PV pattern R (1, 2, 1.5), which is located at (p, y) = (3.25, 2.375), is in range of 12–15. Thus the searching time is in range of 120–150 ms.

If the dither is random noise with sampling period of 10 ms (see Fig. 8e), then the GMPP is also found. So, the proposed aPSCH1 scheme may use the inherent ripple from the inverter inputs (voltage or current). The dither gain (G_d) and p_1 and p_2 components (mentioned in Fig. 1) are also shown in Fig. 8. The average value of the p_1 component (p_{1av}) over a sampling period is shown in Fig. 8e – last plot in order to highlight the searching of GMPP after passing through the LMPPs.

Discussion

The aPESC scheme is tested here to evaluate the performance of locating, searching and tracking of the Global Maximum Power Point (GMPP). So, the PV applications are the main field of use [30,31], but this aPESC scheme can be also used for Fuel Cell (FC) applications [32] because will reduce the FC power ripple [33] that may damage the FC membrane and reduce the efficiency as well [34].

If two aPESC schemes will be used, one for the PV panel and second for the FC stack, then high energy efficiency can be obtained for Hybrid Power Sources (HPS) [35,36] by harvesting the available energy from both energy sources [37].

Please cite this article in press as: Bizon N, Kurt E, Performance analysis of the tracking of the global extreme on multimodal patterns using the Asymptotic Perturbed Extremum Seeking Control scheme, International Journal of Hydrogen Energy (2016), http://dx.doi.org/10.1016/j.ijhydene.2016.11.173

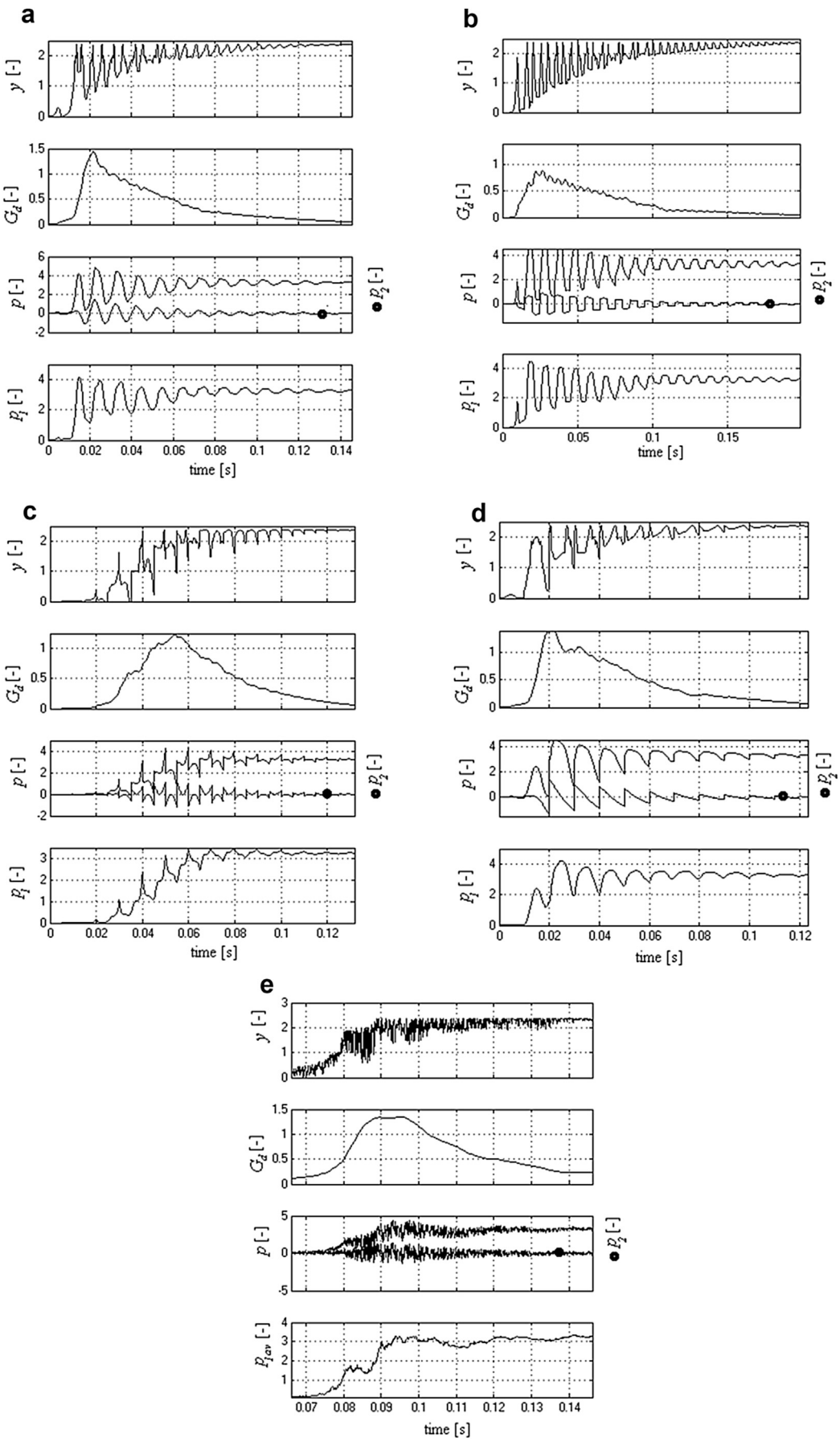

Fig. 8 – Robustness to dither's shape. a. Sinusoidal dither. b. Rectangular dither (50% duty cycle). c. Combination of sinusoidal and rectangular dither. d. Saw-tooth dither. e. Random noise (sampling period of 10 ms).

Please cite this article in press as: Bizon N, Kurt E, Performance analysis of the tracking of the global extreme on multimodal patterns using the Asymptotic Perturbed Extremum Seeking Control scheme, International Journal of Hydrogen Energy (2016), http://dx.doi.org/10.1016/j.ijhydene.2016.11.173

So, the performance and robustness of the aPESC scheme may be further analyzed for different energy sources used in HPS for mobile and stationary applications [37] or in distributed generation [33].

Conclusions

In this paper the performance indicators used to compare the GMPPT algorithms (searching resolution, tracking accuracy, tracking efficiency, and tracking speed) are evaluated for the aPESCH1 scheme proposed here. The performance obtained is given by 100% hit count for 6.25% searching resolution or lower, 99.99% tracking accuracy for stationary regime, tracking speed of maximum 15 iterations, and about 99.96% tracking efficiency.

The simulation shown that 100% hit count may also be obtained for lower R_S that 6.25%, but higher than 0.25%.

The robustness of the aPESCH1 scheme was shown using a dynamic sequence of three PV patterns, where the GMPP is located in right, middle and left side of these patterns. The GMPP of noiselessly PV patterns was accurately tracked. The robustness of the GMPP searching for noisy PV patterns is also shown. The GMPP with random noise added is continuously tracked.

The robustness analysis to dither shape reveals that the shape of the dither is not important and the performance remains almost the same. Besides the shape of sinusoidal, rectangular, combination of sinusoidal and rectangular signals, and saw-tooth, the random noise with sampling period of 10 ms is used as dither. So, the inherent ripple on the DC bus of the inverter may be used as dither as well.

Acknowledgements

The research that led to the results shown here has received funding from the research projects "Cost-Efficient Data Collection for Smart Grid and Revenue Assurance (CERA-SG)", ID: 77594, 2016-19, ERA-Net Smart Grids Plus, "Experimental validation of a propulsion system with hydrogen fuel cell for a light vehicle – Mobility with Hydrogen Demonstrator", ID: PN-III P2-2.1-PED-2016-1223, and "System for acquisition, monitoring, analysis and recognition of the vibration protection of critical infrastructure", ID: PN-III-P2-2.1-PTE- 2016-0215, and Erasmus + project "Innovative European Studies on Renewable Energy Systems", ID: 2015-1-TR01-KA203-021342.

REFERENCES

[1] Ariyur KB, Krstic M. Real-time optimization by extremum-seeking control. Hoboken: Wiley- Interscience; 2003.
[2] Tan Y, Nešic D, Mareels I, Astolfi A. On global extremum seeking in the presence of local extrema. Automatica 2009;45(1):245–51.
[3] Esmaeilzadeh Azar F, Perrier M, Srinivasan B. A global optimization method based on multi-unit extremum-seeking for scalar nonlinear systems. Comput Chem Eng 2011;35:456–63.
[4] Bizon N. Energy harvesting from the PV hybrid power source. Energy 2013;52:297–307.
[5] Bizon N. Energy harvesting from the FC stack that operates using the MPP tracking based on modified extremum seeking control. Appl Energ 2013;104:326–36.
[6] Ishaque K, Salam Z. A review of maximum power point tracking techniques of PV system for uniform insolation and partial shading condition. Renew Sustain Energy Rev 2013;19:475–88.
[7] García M, Maruri JM, Marroyo L, Lorenzo E, Pérez M. Partial shadowing, MPPT performance and inverter configurations: observations at tracking PV plants. Prog Photovolt Res Appl 2008;16(6):529–36.
[8] Eltawil MA, Zhao Z. MPPT techniques for photovoltaic applications. Renew Sustain Energy Rev 2013;25:793–813.
[9] Liu Z-H, Chen J-H, Huang J-W. A review of maximum power point tracking techniques for use in partially shaded conditions. Renew Sustain Energy Rev 2015;41:436–53.
[10] Thounthong P, Sikkabut S, Luksanasakul A, Koseeyaporn P, Sethakul P, Pierfederici S, Davat B. Fuzzy logic based DC bus voltage control of a stand alone photovoltaic/fuel cell/supercapacitor power plant. 11th International Conference on Environment and Electrical Engineering (EEEIC) 2012:725–730.
[11] Liao C-C. Genetic k-means algorithm based RBF network for photovoltaic MPP prediction. Energy 2010;35(2):529–36.
[12] Shaiek Y, Smida MB, Sakly A, Mimouni MF. Comparison between conventional methods and GA approach for maximum power point tracking of shaded solar PV generators. Sol Energy 2013;90:107.
[13] Tajuddin MFN, Ayob SM, Salam Z, Saad MS. Evolutionary based maximum power point tracking technique using differential evolution algorithm. Energy Build 2013;67:245–52.
[14] Sarvi M, Ahmadi S, Abdi S. A PSO-based maximum power point tracking for photovoltaic systems under environmental and partially shaded conditions. Prog Photovolt Res Appl 2015;23(2):201–14.
[15] Jianga LL, Maskell DL, Patra JC. A novel ant colony optimization-based maximum power point tracking for photovoltaic systems under partially shaded conditions. Energy Build 2013;58:227–36.
[16] Zhou L, Chen Y, Guo K, Jia F. New approach for MPPT control of photovoltaic system with mutative-scale dual-carrier chaotics search. IEEE Trans Power Electron 2011;26:1038–48.
[17] Thounthong P, Luksanasakul A, Koseeyaporn P, Davat B. Intelligent model-based control of a standalone photovoltaic/fuel cell power plant with supercapacitor energy storage. IEEE Trans Sustain Energy 2013;4(1):240–9.
[18] Ishaque K, Salam Z, Lauss G. The performance of perturb and observe and incremental conductance maximum power point tracking method under dynamic weather conditions. Appl Energy 2014;119:228–36.
[19] Koutroulis E, Kalaitzakis K, Voulgaris NC. Development of a microcontroller- based, photovoltaic maximum power point tracking control system. IEEE Trans Power Electron 2001;16:46–54.
[20] Orioli A, Di Gangi A. Review of the energy and economic parameters involved in the effectiveness of grid-connected PV systems installed in multi-storey buildings. Appl Energy 2014;113:955–69.
[21] Patel H, Agarwal V. MPPT scheme for a PV-fed single-phase single-stage grid-connected inverter operating in CCM with only one current sensor. IEEE Trans Energy Convers 2009;24:256–63.
[22] Bahgat ABG, Helwa NH, Ahmad GE, El Shenawy ET. Maximum power point tracking controller for PV systems using neural networks. Renew Energy 2005;30:1257–68.

Please cite this article in press as: Bizon N, Kurt E, Performance analysis of the tracking of the global extreme on multimodal patterns using the Asymptotic Perturbed Extremum Seeking Control scheme, International Journal of Hydrogen Energy (2016), http://dx.doi.org/10.1016/j.ijhydene.2016.11.173

[23] Silvestre S, Chouder A. Effects of shadowing on photovoltaic module performance. Prog Photovoltaics Res Appl 2008;16(2):141–9.
[24] Jiang J-A, Liang Y-T, Wang J-C, Su Y-L, Kuo K-C, Shieh J-C. A novel analytical model for determining the maximum power point of thin film photovoltaic module. Prog Photovolt Res Appl 2014;22(3):318–31.
[25] Durán E, Andújar JM, Galán J, Sidrach-de-Cardona M. Methodology and experimental system for measuring and displaying I–V characteristic curves of PV facilities. Prog Photovolt Res Appl 2009;17(8):574–86. http://dx.doi.org/10.1002/pip.909.
[26] Nguyen TL, Low KS. A global maximum power point tracking scheme employing DIRECT search algorithm for photovoltaic systems. IEEETrans Ind Electron 2010;57:3456–67.
[27] Patel H, Agarwal V. Maximum power point tracking scheme for PV systems operating under partially shaded conditions. IEEE Trans Ind Electron 2008;55:1689–98.
[28] Liu YH, Huang SC, Huang JW, Liang WC. A particles warm optimization-based maximum power point tracking algorithm for PV systems operating under partially shaded conditions. IEEE Trans Energy Convers 2012;27:1027–35.
[29] Tan T, Dragan N, Iven M. On the choice of dither in extremum seeking systems: a case study. Automatica 2008;44:1446–50.
[30] P Mungporn, S Sikkabut, B Yodwong, C Ekkaravarodome, S Toraninpanich, B Nahid-Mobarakeh, S Pierfederici, B Davat, P Thounthong. Photovoltaic power control based on differential flatness approach of multiphase interleaved boost converter for grid connected applications. International Conference on Clean Electrical Power (ICCEP), 2015, 574–579.
[31] Bouzelata Y, Kurt E, Chenni R, Altın N. Design and simulation of a unified power quality conditioner fed by solar energy. Int J Hydrogen Energ 2015;40(44):15267–77.
[32] Thounthong P, Raël S, Davat B. Control strategy of fuel cell and supercapacitors association for a distributed generation system. IEEE Trans Industrial Electron 2007;54(6):3225–33.
[33] Bizon N, Tabatabaei NM, Shayeghi H. Analysis, control and optimal operations in Hybrid power systems – advanced techniques and applications for linear and nonlinear systems. London, UK: Springer Verlag London Limited; 2013.
[34] Thounthong P, Davat B, Raël S, Sethakul S. Fuel cell high-power applications. IEEE Ind Electron Mag 2009;3(1):32–46.
[35] Madaci B, Chenni R, Kurt E, Hemsas KE. Design and control of a stand-alone hybrid power system. Int J Hydrogen Energ 2016;41(29):12485–96.
[36] Thounthong P, Sikkabut S, Mungporn P, Piegari L, Nahid-Mobarakeh B, Pierfederici S, et al. DC bus stabilization of Li-Ion battery based energy storage for a hydrogen/solar power plant for autonomous network applications. IEEE Trans Industry Appl 2015;51(4):2717–25.
[37] Bizon N, Oproescu M, Raceanu M. Efficient energy control strategies for a standalone renewable/fuel cell hybrid power source. Energy Convers Manag 2015;77:768–72.

Please cite this article in press as: Bizon N, Kurt E, Performance analysis of the tracking of the global extreme on multimodal patterns using the Asymptotic Perturbed Extremum Seeking Control scheme, International Journal of Hydrogen Energy (2016), http://dx.doi.org/10.1016/j.ijhydene.2016.11.173